Int. J. Electrochem. Sci., 16 **(2021)** Article ID: 210567, doi: 10.20964/2021.05.67

International Journal of
ELECTROCHEMICAL
SCIENCE
www.electrochemsci.org

Electrochemical Behaviour and X-ray Fluorescence Study of AgNP-GO-CS Coated AISI 303 Austenitic Stainless Steel and Ceramic Commercial Products

Sabreen A. Baioumy[1,2], *Wafaa A. Sanad*[3], *Ahmed A. El-Sherif*[1], *Amany M. Fekry*[1,4], *Lev O. Filippov*[4,5*]

[1] Chemistry Department, Faculty of Science, Cairo University, 12613 Giza, Egypt
[2] Chemical Testing Laboratories, Egyptian Organization for Standardization & Quality (EOS), Cairo, Egypt
[3] Hot Lab Center, Chemistry Department, Atomic Energy Authority, Egypt
[4] Université de Lorraine, CNRS, GeoRessources, F-54000 Nancy, France
[5] National University of Sciences and Technology MISIS, 4 Leninsky Prospekt, 119049 Moscow, Russia
[*]E-mail: Amanym.Fekry@gmail.com

Received: 27 December 2020 / *Accepted:* 18 February 2021 / *Published:* 31 March 2021

Herein, the performance of stainless steel and ceramic commercial cooking utensils was investigated under varying temperature, hydrogen evolution and pH. X-ray fluorescence (XRF) analysis was used to determine the elemental composition of commercial products manufactured by a local company. Prior to XRF analysis, the products were immersed in universal buffer for 2 days at different pH and temperature values before and after coating with silver nanoparticles/graphene oxide/chitosan. Release assessments were performed for both types of commercial utensils. Total reflection XRF was used to precisely examine the wt% of Cr, Mn, and Ni for the stainless steel sample and Si, Ti, and Ba for the ceramic sample after immersion under certain conditions. The ion release from both materials was temperature- and pH-dependent before and after nanocoating. All experiments showed that the lowest hydrogen evolution and amount of release for both commercial utensils occurred at low temperature and high pH values with this nanocoating. The coatings were also studied electrochemically; the stainless steel was more passive than the ceramic without coating. After coating, they were comparable at temperatures of 75 - 250 ^{o}C from pH 5 - 11, where the ceramic performed better than the stainless steel and was more passive. The novel nanocoating reported in this work will enable both customers and manufactures to upgrade the quality of their products.

Keywords: Ceramic; Stainless steel; XRF; utensils; nanocoating

1. INTRODUCTION

X-ray fluorescence (XRF) is a fast, accurate and non-deteriorating technique with detection limit in the order of ppm for different elements [1,2]. Therefore, XRF analysis is extensively utilised in various fields, especially in the food industry.

Ceramic materials [3] are unique because of their exceptional properties, such as low electrical and thermal conductivity. Therefore, owing to which they are extensively used in numerous areas. XRF techniques can be employed to examine the corrosion difficulties that occur in ceramics as recently done in several studies on food interaction [4,5].

Stainless steel is commonly used to manufacture cooking utensils and kitchen tools owing to its high corrosion resistance [6-10]. Austenitic steel is most widely used in utensils, and the AISI 303 alloy is permitted for use with food [11,12]. However, AISI 303 austenitic releases a higher amount of Mn than other known stainless steel [13]. To minimize metal transfer to food, utensils are often covered with a coating such as silver nanoparticles, chitosan and graphene oxide nanoparticles. If these metals and alloys are not shielded, metal ions may migrate into food, leading to negative effects on human health [14].

The analysis of steel or ceramic is beneficial for numerous purposes [15]. However, most analyses include only the standard wet chemical method or inductively coupled plasma atomic emission, which are unhelpful [16]. The XRF technique is practical in several areas, particularly for metal and alloy analyses [1, 17]. Sample preparation for XRF is relatively simple and requires less time and effort [18].

Temperature and pH are critical parameters that govern the type of alloy that can be used in utensil production [19]. High temperatures may increase the metal corrosion that occurs upon contact with food, resulting in a high percentage of toxicity. Moreover, food consists of proteins, carbohydrates, fats and other compounds, which have a wide pH range that impacts food corrosivity [20], significantly influencing cooking utensils. Several studies have been published on the release of alloy elements into different food and food simulators [11,21,22].

In this study, we tested commercial cooking utensils by covering them with a coating that is safe for human health. A novel nano-coating consisting of silver nanoparticles (AgNPs), graphene oxide (GO) and Chitosan (CS) polymer was applied on stainless steel and ceramic utensils at various temperature and pH values to test its potential use for industrial application. CS is a natural non-toxic polymer [23-24], AgNPs are safe and non-toxic [25-26], GO was utilized to strengthen the nano-coating [27]. The elemental composition of the stainless steel and ceramic commercial utensils, both coated and uncoated, was determined by XRF after exposure to different pH (simulated food contact) and temperatures. In addition, different electrochemical techniques were used to study the two materials before and after coating to ensure sufficient protection using this novel nano-coating.

2. MATERIALS AND METHODS

2.1. Preparation of samples

Stainless steel and ceramic samples were cut from pans obtained commercially from a famous supermarket in Egypt; the compositions are listed in Tables 1 and 2, respectively. The sample composition of the stainless steel and ceramic was measured by XRF. The samples were cut from the flat portion of each pan in the form of a disc with a diameter of 40 mm.

Table 1. Chemical composition of stainless steel pan by XRF.

Elements	Fe	Cr	Ni	Mn	Si	Mo	Al	V	Mg
Wt%	69.7	18.22	8.9	1.31	0.44	0.23	0.13	0.09	0.04

Table 2. Chemical composition of ceramic pan by XRF.

Elements	Si	Ti	Ba	Fe	Mn	Al	Mg	Cr	Ni
Wt%	68.2	19.14	8.9	0.74	0.5	0.3	0.25	0.14	0.04
Wt%									

2.2. Chemicals and reagents

CS from crab shells (85% deacetylated) and graphite powder were purchased from Sigma-Aldrich, USA. $AgNO_3$ was purchased from Merck. Glutaraldhyde, KNO_3, NaOH, phosphoric acid, glacial acetic acid and boric acid were used as analytical reagents.

The universal buffer used [28,29] comprised a 100 mL mixture of acids: 0.04 M phosphoric acid, 0.04 N acetic acid, 0.04 N boric acid and was adjusted to the required pH (2.0-11) using 0.2 N sodium hydroxide.

2.3. Instrumentation

2.3.1. Apparatus

All voltametric measurements were performed using an SP 150 potentiostat/galvanostat (Bio-Logic Science) workstation. The three electrodes were connected toan electrochemical workstation.

Electrochemical impedance spectroscopy measurements were performed at an AC amplitude of 10 mV in the frequency range of 100 mHz to 100 kHz. Data fitting was performed using EC-Lab® software. The potentiodynamic polarisation curves were measured from -1.0 V to 0.4 V (SCE) at a scan rate of 1 mV/s after immersing the samples in the test solutions for 3 h to obtain a stable open circuit potential.

2.3.2. S8 TIGER-Spectrometer

A Bruker high performance sequential wavelength-dispersive XRF (S8 TIGER) was used for universal qualitative, quantitative and "standard-less" multi element analysis of the elements (depending on the optional spectrometer configuration), ensuring a non-destructive and ecologically safe analytical process. The S8 TIGER spectrometer is widely used in process control, quality control, research and development, and Monitoring; its robust, dirt-resistant design ensures efficient analysis even under extreme conditions with a 4 Kw high-power XRF.

2.3.3. Chillo Baths NB7 series

The Chillo bath contained two components a thermo-circulator which provided temperature control while simultaneously stirring/mixing liquids in the bath, and external circulation. The thermo-circulator was fitted onto a compressor cooling system comprising a stainless steel tank above a refrigeration compressor, which operates at ambient pressure from -20 °C to 130 °C.

2.3.4. pH meter

An Adwa 1030 digital pH meter (Romania) linked to glass electrode was used to measure the pH.

2.4. Methods

2.4.1. Alloy Evaluation

Stainless steel and ceramic samples with a diameter of 40 mm were used. Universal buffer solutions of different pH values were prepared. The samples were subjected to various conditions, such as different pH values (2–11) and different temperatures (10–250 °C) using Chillo baths.

A commercially available ceramic pan was evaluated for particle migration under used conditions. The migration of Ti, Si, and Ba was evaluated using buffer solutions with different pH values and temperatures.

The same experiments were repeated for a stainless steel pan (commercially available). The migration of Fe, Cr, and Ni was evaluated under the same conditions.

2.4.2. Deposition of the Coating

CS gel was prepared by adding 0.50 g of CS to 98.0 mL of water and 2.0 mL of glacial acetic acid to attain a pH of approximately 3 and stirring for 2 h [30]. GO was prepared from graphite powder using a modified Hummer's method [31] after which the prepared GO (0.5 g) was dispersed in 30 mL of the prepared chitosan solution with ultrasonic stirring for 20 min. An aqueous solution of 10^{-3} M $AgNO_3$ in 0.1 M KNO_3 was added to the GO/CS solution under stirring. Subsequently, a potential of -

0.4 V was applied for 2 min to form AgNPs [32], and the films were precipitated on the sample surface (stainless steel or ceramic) to form the final AgNP/GO/CS nanocomposites.

2.4.3. Coating characterization and electrochemical study

A JEOL JXA-840A scanning electron microscope combined with an energy-dispersive X-ray spectroscopy (EDX) unit for elemental analysis was used for the characterisation of the coating.

3. RESULTS AND DISCUSSION

3.1. XRF analysis

The effects of temperature (10–250 °C) and pH on the stainless steel alloy are displayed in Figure 1a–e. The elemental percentage of metals (Fe, Cr, and Ni) on the alloy surface increased with increasing pH of the medium from acidic to basic. This may be attributed to the initial formation of oxides, followed by the formation of hydroxides of the metal ions at the highest pH of 11. However, the elemental percentage decreased with increasing temperature, indicating that high temperature deteriorated the stainless steel.

Corrosion resistance is a significant property of austenitic stainless steel owing to the development of passive films of Cr_2O_3, NiO, and iron oxides at low pH values, followed by those of $Cr(OH)_3$, $Ni(OH)_2$, and iron hydroxides at higher pH [33,34]. The passive film thickness decreases with decreasing pH [34]. Thus, increasing the solution pH is beneficial for creating passive films with better shielding behaviour [35].

In practice, varying the pH has a noteworthy effect on the corrosion behaviour of stainless steel [36]. Increasing the pH leads to a thickening of the nanocoating, mainly because of the stabilisation of iron oxides in basic solutions. In acidic solutions, a chromium-rich oxide film is formed because of the slower dissolution rate of chromium oxide than that of iron oxide [37,38]. A low pH was found to have a significant effect on the corrosion behaviour of stainless steel [36,39] with a low hydrogen evolution rate.

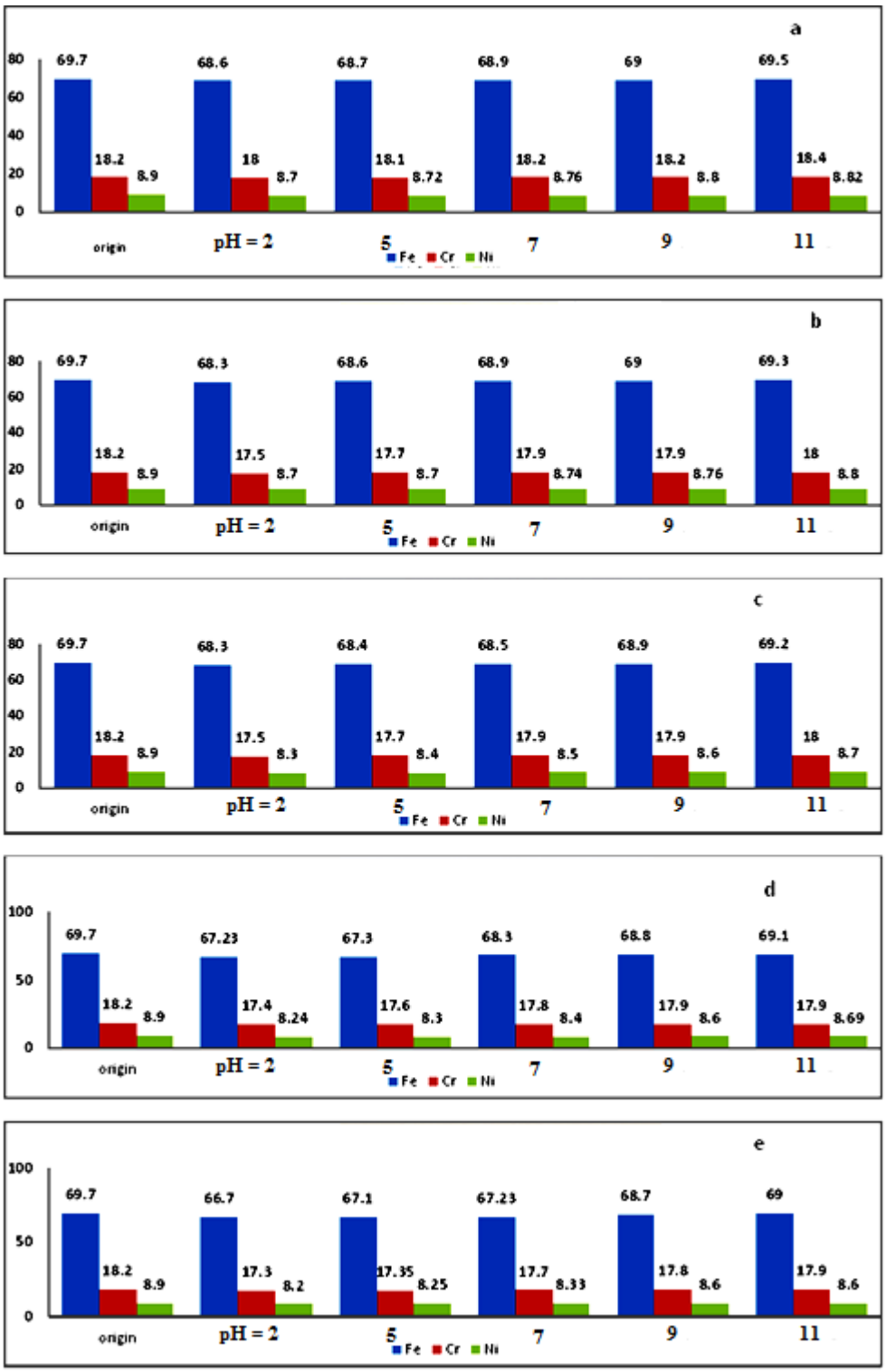

Figure 1. XRF results for stainless steel alloy at different pH values and temperatures a) 10 ºC; b) 50 ºC; c) 100 ºC; d) 150 ºC and, F) 250 ºC; after immersion in universal buffer for 2 days.

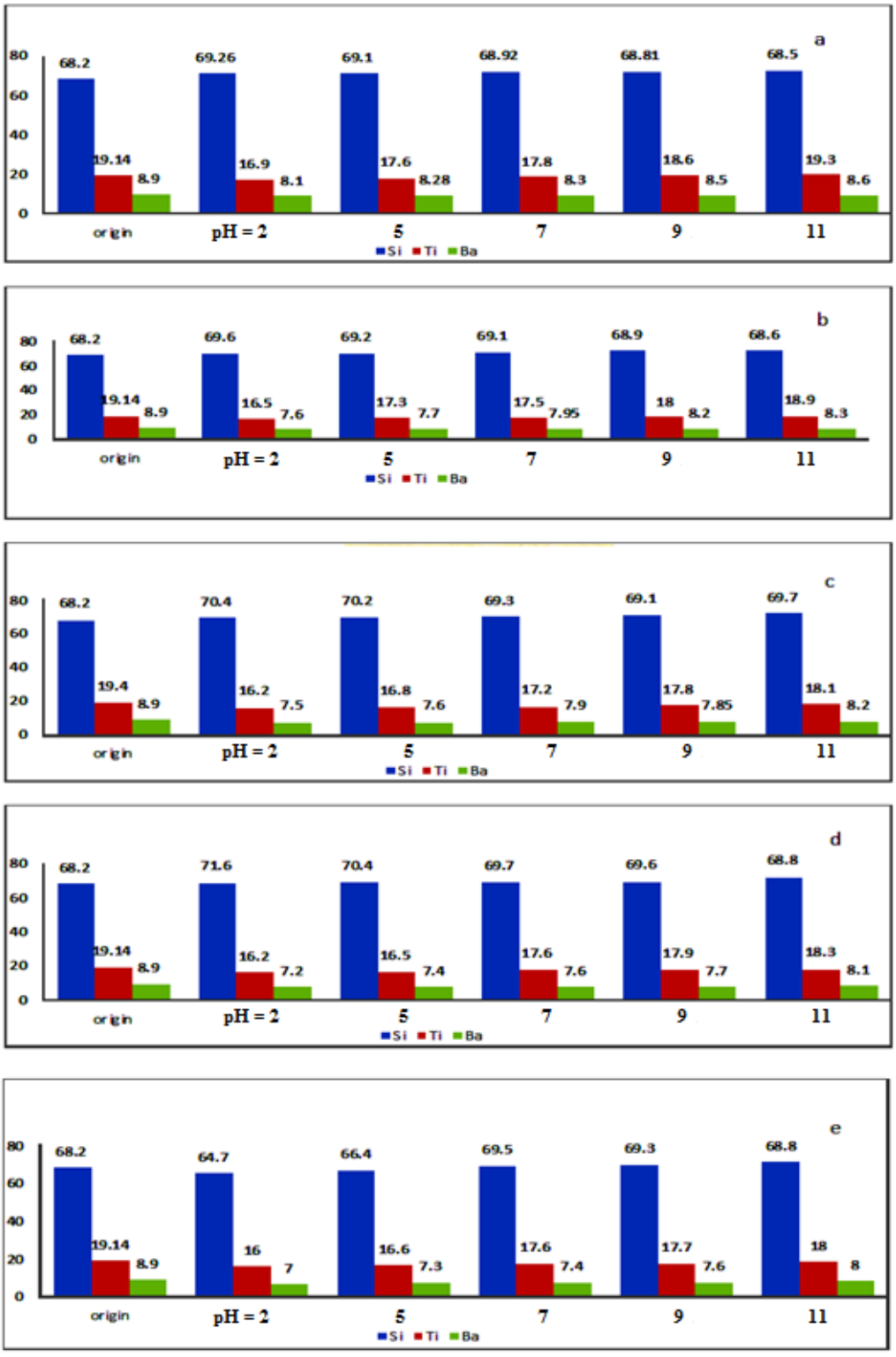

Figure 2. XRF results for ceramic samples at different pH values and temperatures of a) 10 °C, b) 50 °C, c) 100 °C, d) 150 °C, and e) 250 °C after immersion in universal buffer for 2 days.

Figure 2a–e display the effect of temperature from 10 to 250 °C along with the influence of pH on the ceramic material. The wt% of Si was stable over all investigated pH values and temperatures

due to the formation of a passive layer, except at 250 °C for the pH values of 2 and 5, where the wt% first decreased and then increased with increasing pH. The wt% of Ti and Ba on the ceramic surface first decreased at low pH values of 2 and 5 and then increased from a pH of 7 onwards over all investigated temperatures.

However, the elemental percentage decreased with increasing temperature, and it was observed that the temperature deteriorated the ceramic by a lower percentage than that of stainless steel. This is because the elements that comprise the ceramic are higher in passivity than those present in the stainless steel. Titanium plays a major role in improving the chemical stability of the ceramic and improving its microstructure with increasing pH (lower hydrogen evolution) by forming titania [40,41].

Generally, it was found that the release of elements from both tested materials decreased owing to the high adsorption of chitosan on the material surface [41]. The addition of GO strengthened the film and significantly decreased surface corrosion. Finally, adding AgNPs [25] to the coating further decreased the release of elements because the NPs increased the effective surface area of the coating, covering more of the surface of the stainless steel and ceramic samples. This suggests that both types of materials when coated with AgNP/GO/CS can be used safely at all pH values and temperatures up to 250 °C. Therefore, this coating can be used industrially as a safe and environmentally friendly nanocoating.

3.2. SEM and EDX analysis

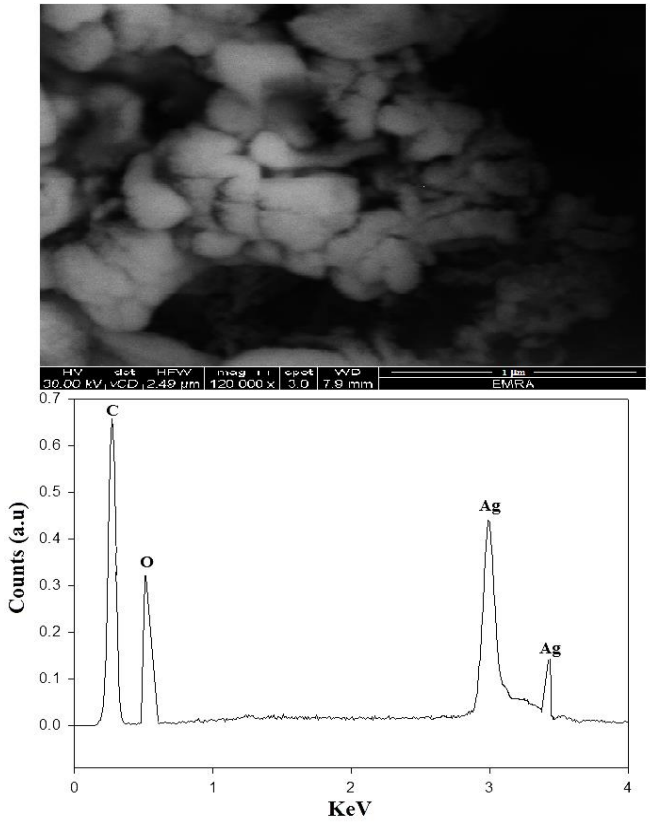

Figure 3. SEM and EDX results for AgNP/GO/CS nanocomposite.

Figure 3 shows the SEM and EDX results of the nanocoating. An thich crystalline compact film is observed in the SEM image, where GO and AgNPs are densely packed within the chitosan matrix. The EDX analysis confirmed the formation of the nanocoating. This nanocoating ensures high protection performance in both types of utensils and retains its protection capability even at high temperatures [44,45].

3.3. Impedance and polarisation measurements

3.3.1. Effect of temperature and pH

Figure 4a and b show the Bode plots for the stainless steel alloy at 250 °C. The inset shows the polarisation curves at the same temperature. The AgNP/GO/CS coated materials were established, and the effects of different pH values (2, 7, and 11) on the samples at 250 °C are summarized in Tables 3 and 4 for the stainless steel and ceramic samples, respectively. Fig. 5 shows the model circuit that fits [46–50] these data, which are provided in Tables 3 and 4. The model is a two time constant model with an internal oxide layer whose capacitance and resistance are denoted by Q_1 and R_1, respectively. Q_2 and R_2 correspond to the external layer capacitance and resistance, respectively. Q is introduced to account for the non-surface homogeneity [51–54].

For the polarisation data, the electrochemical parameters (corrosion potential (E_{corr}) and corrosion current density (i_{corr})) were obtained by extrapolation of the Tafel curves. The anodic branch indicates film breakdown, and the cathodic branch indicates hydrogen evolution ($H_2\uparrow$) [55]. The potential showed a positive shift with increasing pH (bare or coated surface). In addition, the hydrogen evolution rate increased with decreasing pH values.

The data in Tables 3 and 4 show that the impedance value is lower for the bare surfaces of both types of materials compared to the coated ones. At low pH, the hydrogen evolution rate is high, and H^+ ions destabilise the passive layer on both materials. Thus, the impedance value and phase angle maximum were lowest at pH 2 and highest at pH 11.

The impedance value for the AgNP/GO/CS nanocoating was sufficiently high even at 250 °C in comparison to previously published electrochemical results [44,45] owing to the high degree of surface coverage with the nanocoating even at high temperatures. In addition, the film provided a large surface area due to the nanoparticles of silver and also AGNPS imparting a shiny colour to both material surfaces.

Thus, the optimal pH value was 11 with the lowest hydrogen evolution rate, which indicates an improvement in the corrosion resistance with the nanocomposite coating at pH 11.

The protection efficiency was calculated from the polarisation parameters using the following equation [52]:

$$PE\% = (i_{corr} - i_0 / i_0) \times 100 \quad (1)$$

where i_0 and i_{corr} represent the corrosion current densities of the bare and coated specimens, respectively. The PE% values are listed in Tables 3 and 4. Thus, the protection efficiency was the highest for the AgNP/GO/CS nanocomposite at pH 11.

Additionally, the protection efficiency was calculated using the impedance and the following equation [52] and tabulated in Tables 3 and 4:

$$\%PE = \frac{R_{T(inhibited)} - R^{o}_{T(Blank)}}{R_{T(inhibited)}} \quad (2)$$

where R°_{T} and R_{T} are the total resistances of steel in the absence and presence of inhibitors, respectively. These results are comparable with those obtained from the protection efficiency calculated from the polarisation.

The corrosion or hydrogen evolution on stainless steel may be due to the reaction of the buffer with iron in the stainless steel:

Anodic reaction (Oxidation reaction)

$Fe \rightarrow Fe^{2+} + 2e^{-}$ (3)

Cathodic (Reduction reaction or hydrogen evolution reaction)

$2H^{+} + 2e^{-} \rightarrow H_2\uparrow$ (4)

The proposed mechanism at low pH is the Volmer reaction (slow step) as the primary discharge step, $M + H_3O^{+} + e^{-} \leftrightarrow MH_{ad} + H_2O$, the Heyrovsky reaction (fast step) as the second step, followed by an electrochemical desorption step, $MH_{ad} + H_3O^{+} + e^{-} \rightarrow M + H_2 + H_2O$. The final step is the Tafel reaction (fast step), a recombination step, $MH_{ad} + MH_{ad} \rightarrow 2M + H_2$. Therefore, the hydrogen evolution reaction occurs in three steps. If the Volmer reaction is fast, the Tafel and/or Heyrowsky reaction must be slow, and vice versa [55].

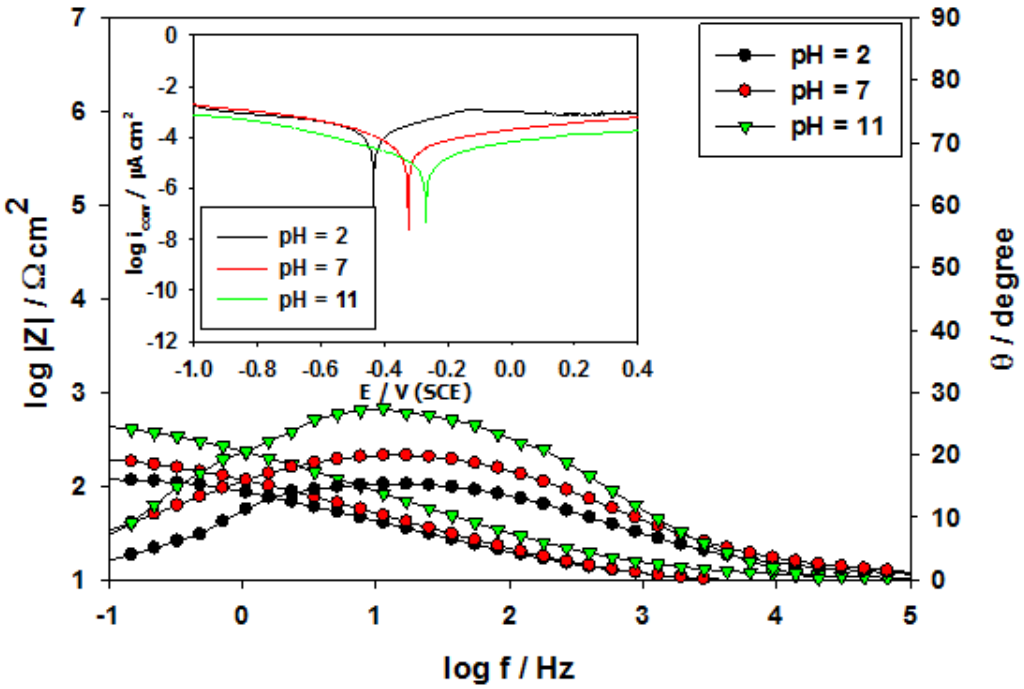

Figure 4. Bode plots for AgNP/GO/CS nanocomposite-coated stainless steel after immersion in universal buffer solution for 3 h at 250 °C (inset shows Tafel plots).

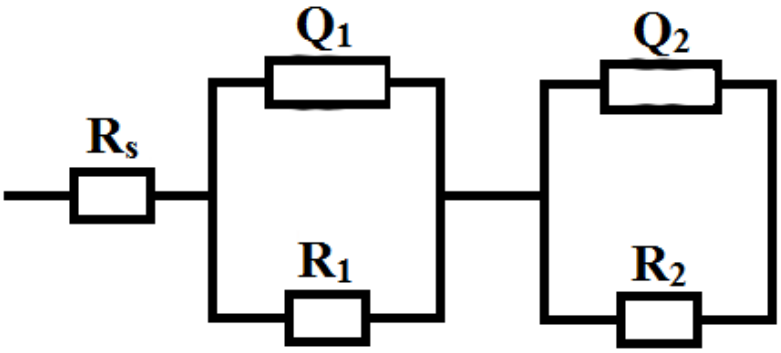

Figure 5. Equivalent circuit for fitting of impedance results.

Finally, the behaviour of the AgNP/GO/CS coating at different pH values in a universal buffer solution at 250 °C (oven temperature) is shown in Figure 4. The coating behaviour is satisfactory up to pH values as low as 2 and temperatures as high as 250 °C. Polarisation data and impedance data are in good agreement, as shown in Tables 3 & 4. The current density decreases and the impedance value increases with increasing pH. Thus, this coating at 250 °C exhibited the lowest impedance or highest current density while maintaining its stability.

Table 3. Polarisation and impedance parameters for bare stainless steel and AgNP/GO/CS nanocomposite coated stainless steel after immersion in universal buffer solution for 3 h at 250 ^{o}C.

Temp (^{o}C)	Electrode	pH	I_{corr} (μA/cm^2)	E_{corr} (v)	PE_{pol} (%)	R_T (kΩ cm^2)	PE_{imp}(%)
250	Bare	pH 2	1876	-0.617	-	0.252	-
		pH 7	1393	-0.511	-	0.550	-
		pH 11	656.0	-0.323	-	1.380	-
250	AgNP/GO/CS	pH 2	531.0	-0.436	71.7	0.871	71.1
		pH 7	370.7	-0.320	73.4	1.995	72.4
		pH 11	113.7	-0.268	82.7	6.310	78.1

Table 4. Polarisation and impedance parameters for bare stainless steel and AgNP/GO/CS nanocomposite coated ceramic after immersion in universal buffer solution for 3 h at 250 ^{o}C.

Temp (^{o}C)	Electrode	pH	I_{corr} (μA/cm^2)	E_{corr} (v)	PE_{pol} (%)	R_T (kΩ cm^2)	PE_{imp} (%)
250	Bare	pH 2	1998	-0.982	-	0.186	-
		pH 7	1481	-0.980	-	0.257	-
		pH 11	811.0	-0.963	-	0.562	-
250	AgNP/GO/CS	pH 2	610.4	-0.691	69.5	0.631	70.5
		pH 7	315.9	-0.643	78.7	1.000	74.3
		pH 11	110.1	-0.582	86.4	3.163	82.2

4. CONCLUSIONS

In this study, we examine the concentration of metals in stainless steel and ceramic pans before and after immersion in buffer solutions with different temperature and pH values. The stainless steel and ceramic pans had the lowest corrosion rate at high pH and low temperature, however; the ceramic pan was more stable than the stainless steel pan, especially at pH > 7 at all temperatures.

The release of metal ions was higher at lower pH values because of the aggressiveness of the medium and high hydrogen evolution. In addition, high temperatures increased the deterioration of both stainless steel and ceramic. The ceramic was more stable at high temperatures than the stainless steel alloy.

Our results demostrate that the proposed procedure for analyzing the wt% of metals using XRF analysis is reliable, and it may be useful to determine the composition of materials used for food manufacturing cooking utensils.

It was found that the percentage release of elements in both types of utensils decreased more with the AgNP/GO/CS nanocoating than with GO/CS or chitosan on the material surface. This indicates that both stainless steel and ceramic utensil coated with the AgNP/GO/CS coating can be used at all pH values and temperatures up to 250 ^{o}C. Thus, this coating can be used industrially as a safe and environmentally friendly nanocoating.

Electrochemical studies on the effect of temperature up to 250 ^{o}C (oven temperature) and that of pH as low as 2, demonstrated a stable coating behaviour with a reliable impedance value.

CONFLICT OF INTEREST
The authors declare no conflict of interest.

References

1. M.A. Al-Eshaikh, A. Kadachi, J**.** King Saud Univ. – Eng. Sci., 23(2011)75-79.
2. H. Ida, T. Segawa, S. Tohyama, J. Kawai, Spectrochimica Acta Part B Atomic Spectroscopy, 60 (2005) 249-252.
3. P.N. Sudha, K. Sangeetha, A.V. Jisha Kumari, N. Vanisri, K. Rani. "Corrosion of ceramic materials", In book: Fundamental Biomaterials: Ceramics, Edition: First edition, Publisher: Elsevier, Editors: Sabu Thomas, Preetha Balakrishnan, M.S. Sreekala, 2018.
4. Z.h. Dong, Li-xin Lu, Zhi-gang Liu, *Packag. Technol*. Sci., 28 (2015) 545–556.
5. S. Ntim, S. Norris, K. Scott, T.A. Thomas, G.O. Noonan, *Food Control,* 87(2018).
6. J.Z. Lu, W.W. Deng, K.Y. Luo, L.J. Wu, H.F. Lu, *Mater. Charact.,* 125 (2017) 99–107.
7. E. Norouzi, M. Atapour, M. Shamanian, *J. Alloys Compd.,* 701 (2017) 335–341.
8. M. Desormeaux, B. Rouxel, A.T. Motta, M. Kirk, C. Bisor, Y. de Carlan, A. Legris, *J. Nucl. Mater.,* 475 (2016) 156–167.
9. S. Sabooni, F. Karimzadeh, M.H. Enayati, A.H.W. Ngan, H. Jabbari, Gas tungsten arc microstructural and mechanical *Mater. Charact.,* 109 (2015) 138–151.
10. K.H. Lo, C.H. Shek, J.K.L. Lai, *Mater. Sci. Eng. R,* 65 (2009) 39–104.
11. G. Herting, I.O. Wallinder, C. Leygraf, *J. Food Eng.,* 87(2) (2008a) 291-300.
12. I. Wallinder, S. Bertling, D. Kleja, C. Leygraf, *Water Air Soil Pollut.,* 170 (2006) 17-35.
13. R. Dalipi, L. Borgese, A. Casaroli, M. Boniardi, U. Fittschen, K. Tsuji, L.E. Depero, *J. Food Eng.,*

173 (2016) 85-91.
14. Council of Europe Resolution CM/Res on metals and alloys used in food contact materials and articles (2013) 9.
15. X. Hou, Y. He, B.T. Jones, *Appl. Spectrosc. Rev.,* 39 (2004) 1-25.
16. Nham, TranT., Analysis of Metals in High Alloy Steel by ICP-AES. Varian Australia Pty. Ltd., Mulgrave, Victoria, Australia (ICP-6) 1991.
17. M.A. Al-Eshaikh,A. Kadachi, J. King Saud Univ**. –** Eng**.** Sci**.,** 45 (2002) 457–462.
18. A.B. Blank, L.P. Eksperiandova, *X-ray Spectrometry*, 23 (2011) 75-79.
19. E.A. H. Al Zubaidy, F.S. Mohammad, G. Bassioni, *Int. J. Electrochem. Sci.,* 6 (2011) 6424 - 6441
20. Y. Hedberg, X. Wang, J. Hedberg, M. Lundin, E. Blomberg, I.O. Wallinder, *J. Mater. Sci. - Mater. Med.,* 24(2013) 1015-1033.
21. G. Herting, D. Lindstrm, I.O. Wallinder, C. Leygraf, *J. Food Eng.,* 93(2009) 23-31.
22. G. Herting, I.O. Wallinder, C. Leygraf, *Corros. Sci.,* 48 (2006) 2120-2132.
23. A.M. Fekry, A. A. Ghoneim, M.A. Ameer, *Surf. Coat. Tech.* 283 (2014) 126 – 132.
24. M.S. Hussein, A.M. Fekry, *ACS Omega,* 4 (2019) 73-78.
25. A.M. Fekry, *Biosens. Bioelectron*., 87 (2017) 1065-1070.
26. S.M. Azab, H.K.A. Elhakim, A.M. Fekry, *J. Mol. Struct*., 1196 (2019) 647-652.
27. S.M. Azab, A.M. Fekry, *New J. Chem.*, 41 (2017) 11846-11852.
28. Lurie, J. "Handbook of Analytical Chemistry", English translation, Mir Publishers, 263 (1975).
29. S.A. Abdel-Gawad, W.M. Osman, A.M. Fekry, *Surf. Eng,.* 35(2019) 1033-1041.
30. D. Lahiri, F. Rouzaud, S. Namin, K. Keshri, J.J. Valdes, L. Kos, N. Tsoukias, A. Agarwal, *ACS Appl. Mater. Interfaces,* 1 (11) (2009) 2470–2476.
31. A.M. Dimiev, J.M. Tour, *ACS Nano,* 8 (2014) 3060-3068.
32. M. Shehata, S.M. Azab, A.M. Fekry, *Can. J. Chem.,* 98(2020)169-178.
33. G. Karafyllias, A. Galloway, E. Humphries, *Mater. Sci.,* 420–421 (2019) 79-86.
34. M. Ameer, A. Fekry, F. Heakal, *Electrochim. Acta,* 50 (2004) 43–49.
35. Olsson, D. Landolt, *Electrochim. Acta,* 48 (2003) 1093–1104.
36. A. Fattah-alhosseini, S. Vafaeian, *Egypt. J. Pet.,* 24 (2015) 333-341.
37. Cardoso, S.T. Amaral, E.M.A. Martini, *Corros. Sci.,* 50(2008) 2429–2436.
38. Carmezim, A.M. Simoes, M.F. Montemor, M. Da CunhaBelo, *Corros. Sci.,* 47 (2005) 581–589.
39. Ningshen, U.K. Mudali, G. Amarendra, B. Raj, *Corros. Sci.,* 53 (2011) 64–70.
40. S. Heidari, T. Hooshmand, B. Yekta, A. Tarlani, N. Noshiri, M. Tahriri, *Ceram. Int.,* 44 (2018) 11682-11692.
41. A.M. Fekry, *RSC Adv.*, 6 (2016) 20276-20285.
42. M.A. Al-Eshaikh, A. Kadachi, *J. King Saud Univ. Eng. Sci.*, 23(2011), 75-79.
43. E. Margui, I. Queralt, M. Hidalgo, *J. Anal. At. Spectrom.*, 28(2013) 266-273.
44. S.A. Bioumy, R.A. Ahmed, A.M. Fekry, *J. Bio- Tribo-Corros.,* 6 (2020) 78.
45. A.M. Fekry, R.A. Ahmed, S.A. Bioumy, *J. Bio- Tribo-Corros***.,** 6 (2020) 106.
46. A.A. El-Sherif, M.M. Shoukry, M.M.A. Abd-Elgawad, *J. Solution Chem.,* 42 (2013) 412–427
47. M.H. Helal, M.A. Salem, M.A. Gouda, N.S. Ahmed, A.A. El-Sherif, *Spectrochim. Acta, Part A*, 147 (2015) 73.
48. K.S. Essa, M. Elhussein, *J. Appl. Geophy.*, 136 (2017) 445.
49. M. Aljahdali, A.A. El-Sherif, *J. Solution Chem.,* 41 (2012) 1759–1776.
50. A.A. El-Sherif, A. Fetoh, Y.K. Abdulhamed, G.M. Abu El-Reash, *Inorg. Chim. Acta,* 480 (2018) 1–15.
51. A.M. Fekry, S.M. Azab, *Nano-Struct. Nano-Objects,* 21 (2019) 100411.
52. S.M. Azab, M. Shehata, A.M. Fekry, *New J. Chem.*, 43(38) (2019)15359-15367.
53. A.M. Fekry, G.G. Mohamed, F.M. Abou Attia, N.S. Ibrahim, S.M. Azab, *J. Electroanal. Chem.,* 848 (2019) 113305.
54. S.M. Azab, A.M. Fekry, *ACS Omega*, 4 (2019) 25-30.

55. A. Ghoneim, R. Saad, A.M. Fekry, *Int. J. Hydrogen energy,* 45, 46 (2020) 24370-24382.